Cancer Cell, Volume *23*

Supplemental Information

Selective Requirement of PI3K/PDK1 Signaling for Kras Oncogene-Driven Pancreatic Cell Plasticity and Cancer

Stefan Eser, Nina Reiff, Marlena Messer, Barbara Seidler, Kathleen Gottschalk, Melanie Dobler, Maren Hieber, Andreas Arbeiter, Sabine Klein, Bo Kong, Christoph W. Michalski, Anna Melissa Schlitter, Irene Esposito, Alexander J. Kind, Lena Rad, Angelika E. Schnieke, Manuela Baccarini, Dario R. Alessi, Roland Rad, Roland M. Schmid, Günter Schneider, and Dieter Saur

Inventory of Supplemental Information

Supplemental Data

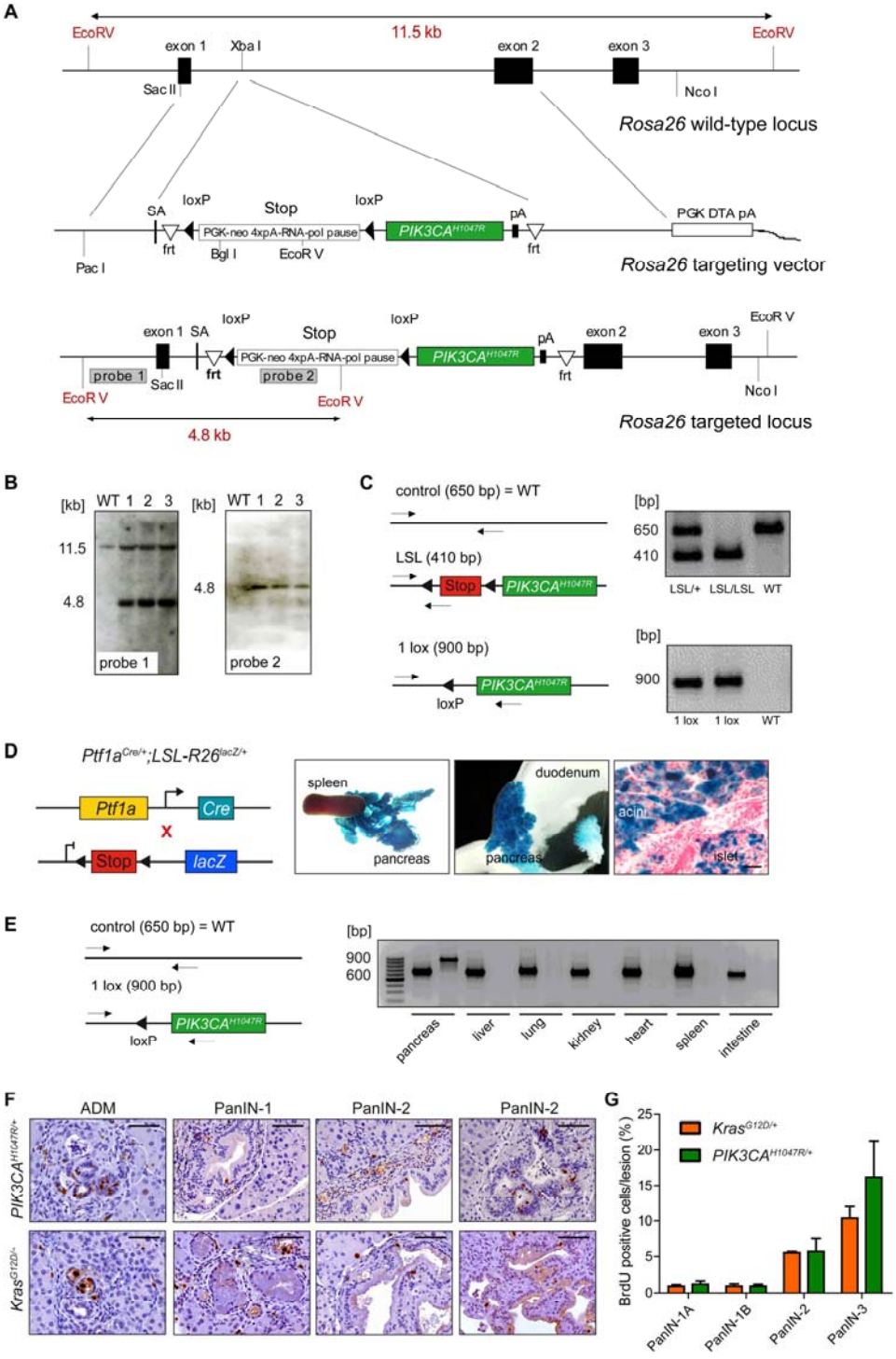

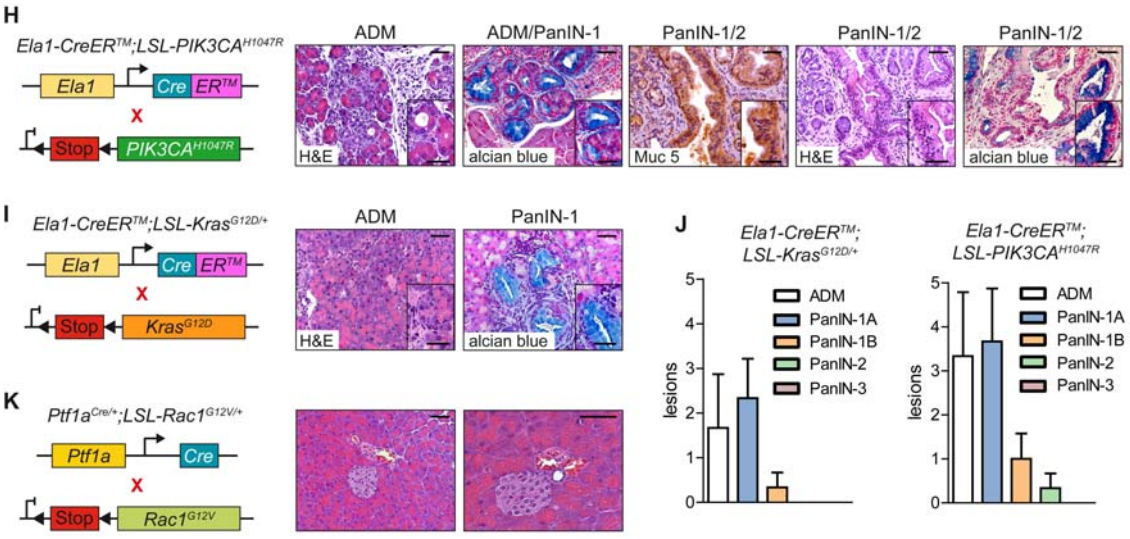

Figure S1, related to Figure 1. Constitutive activation of PI3K, but not Rac1, signaling recapitulates characteristics of Kras^{G12D}-induced PanIN. (A) From top to bottom, diagrams of: *Rosa26* wild-type locus; the *Rosa26* targeting vector with the loxP-stop-loxP (LSL) silenced p110α^{H1047R} (*PIK3CA^{H1047R}*) expression cassette; the targeted *Rosa26* locus. Restriction sites, sizes of DNA fragments and the location of the 5´ (probe 1) and neo (probe 2) probes, are indicated. (B) Southern blot analysis of DNA from wild-type (WT) and targeted embryonic stem cells (1-3) after digestion with EcoRV. The expected bands for the wild-type and targeted alleles are indicated (probe 1 (left panel): WT, 11.5 kb; mutant, 4.8 kb. probe 2 (right panel): WT, no band; mutant, 4.8 kb). (C) Genotyping strategy. PCR analysis of DNA from wild-type (WT), heterozygous (LSL/+) and homozygous (LSL/LSL) *LSL-PIK3CA^{H1047R}* mice with retained stop cassette (upper panel) and DNA extracted from the pancreas of *Ptf1a$^{Cre/+}$;LSL-PIK3CA$^{H1047R/+}$* mice with deleted LSL cassette (1 lox; lower panel). Sizes of WT and mutant PCR products are indicated. (D) Genetic strategy used to analyze pancreas-specific *Ptf1a^{Cre}* mediated recombination with a LSL silenced lacZ reporter line (*LSL-R26$^{lacZ/+}$*). Macroscopic images of whole mount β-galactosidase stained spleen and pancreas (left), small bowel and pancreas (middle), and microscopic images of lacZ activity in pancreatic sections (left). (E) PCR strategy to analyze pancreas-specific *Ptf1a^{Cre}* mediated deletion of the LSL cassette in *Ptf1a$^{Cre/+}$;LSL-PIK3CA$^{H1047R/+}$* mice. Sizes of WT and mutant PCR products are indicated. (F) Representative microscopic pictures of BrdU stained ADM lesions and progressive grades of PanIN lesions of *Ptf1a$^{Cre/+}$;LSL-PIK3CA$^{H1047R/+}$* (upper panel) vs. *Ptf1a$^{Cre/+}$;LSL-Kras$^{G12D/+}$* (lower panel) mice (age from left to right, respectively: 1 month, 3 month, 6 month, 9 month). (G) Quantification of BrdU positive cells in the indicated PanIN lesions of *Ptf1a$^{Cre/+}$;LSL-PIK3CA$^{H1047R/+}$* and *Ptf1a$^{Cre/+}$;LSL-Kras$^{G12D/+}$* mice (n= 3 per time point; 3 representative slides per mouse). (H) Genetic strategy to activate p110α^{H1047R} expression in the acinar compartment of the pancreas (left panel) using *Ela1-CreER^{TM}* mice (no tamoxifen administration; see Fig. 5A-C). Representative H&E, alcian blue and immunohistochemical Muc 5 stains of ADM and PanIN lesions of 12 month old animals (right panel). (I) Genetic strategy used to activate Kras^{G12D} expression in the acinar compartment of the pancreas (left panel). Representative H&E and alcian blue stains of ADM and PanIN lesions of 12 month old animals (right panel). (J) Quantification of ADM and PanINs in 12 month old *Ela1-*

CreER^{TM}*;LSL-Kras*$^{G12D/+}$ and *Ela1-CreER*^{TM}*;LSL-PIK3CA*$^{H1047R/+}$ mice (n = 3 per time point; 3 representative slides per mouse). (K) Genetic strategy used to activate dominant active Rac1^{G12V} expression in the pancreas (left panel). Representative H&E staining of the pancreas of 12 month old *Ptf1a*$^{Cre/+}$*;LSL-Rac1*$^{G12V/+}$ mice (right panel). Insets show representative histology in high magnification. Scale bars, 50 μm for micrographs, 20 μm for insets. Error bars, ±SEM. Note: Due to constitutive Cre activity (see Fig. 5A-C), all *Ela1-CreER*^{TM} animals were analyzed without Cre activation by tamoxifen treatment.

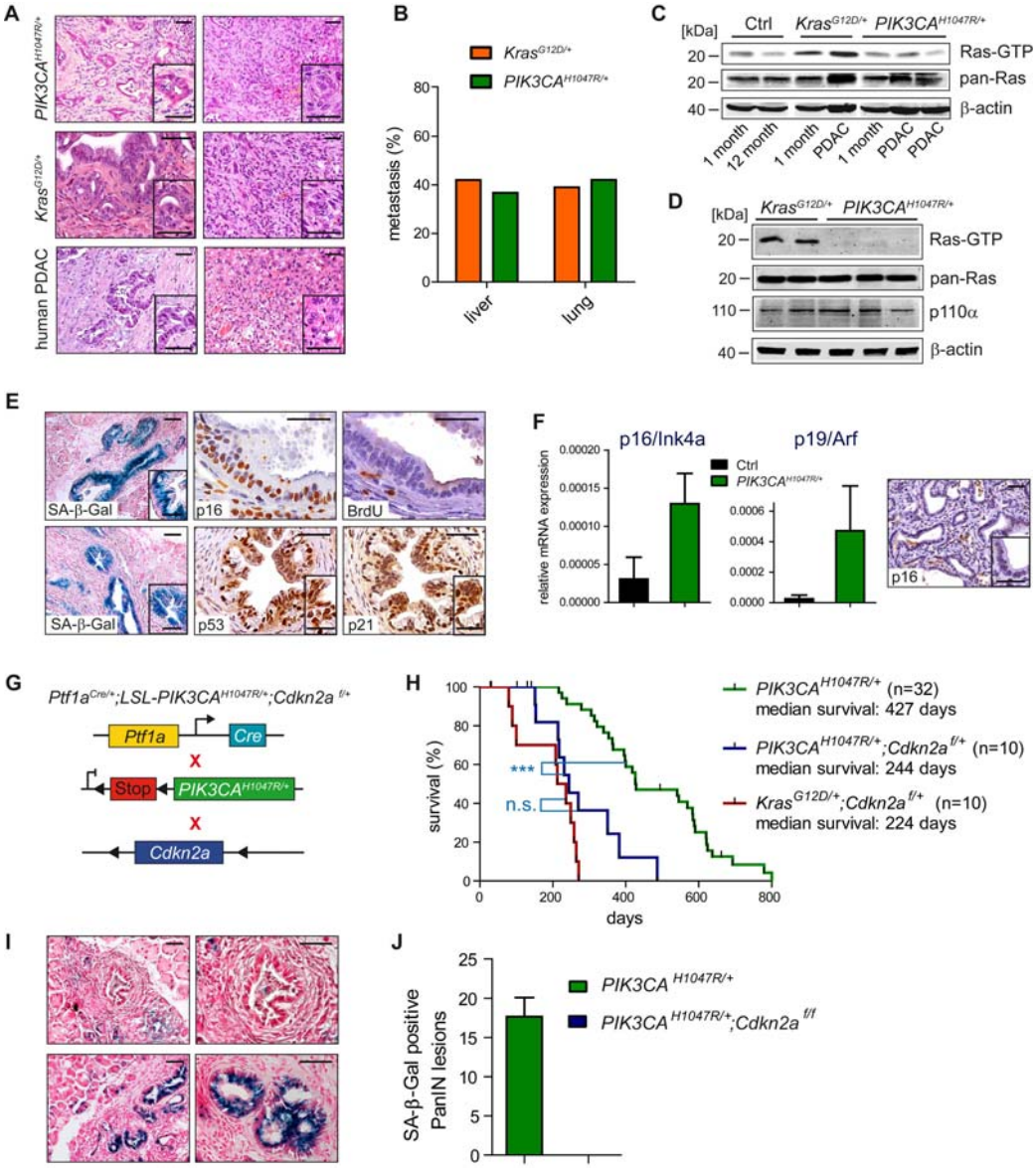
A
PIK3CA H1047R/+
Kras G12D/+
human PDAC
B
Kras G12D/+
PIK3CA H1047R/+
metastasis (%)
liver
lung
C
[kDa]
Ctrl
Kras G12D/+
PIK3CA H1047R/+
Ras-GTP
pan-Ras
β-actin
1 month
12 month
1 month
PDAC
1 month
PDAC
PDAC
D
[kDa]
Kras G12D/+
PIK3CA H1047R/+
Ras-GTP
pan-Ras
p110α
β-actin
E
SA-β-Gal
p16
BrdU
SA-β-Gal
p53
p21
F
p16/Ink4a
p19/Arf
relative mRNA expression
Ctrl
PIK3CA H1047R/+
p16
G
Ptf1a Cre/+;LSL-PIK3CA H1047R/+;Cdkn2a f/+
Ptf1a
Cre
Stop
PIK3CA H1047R/+
Cdkn2a
H
survival (%)
***
n.s.
days
PIK3CA H1047R/+ (n=32)
median survival: 427 days
PIK3CA H1047R/+;Cdkn2a f/+ (n=10)
median survival: 244 days
Kras G12D/+;Cdkn2a f/+ (n=10)
median survival: 224 days
I
J
SA-β-Gal positive PanIN lesions
PIK3CA H1047R/+
PIK3CA H1047R/+;Cdkn2a f/f

Figure S2, related to Figure 2. p110α^{H1047R}- or Kras^{G12D}-induced murine PDAC recapitulates pathologic features of human PDAC. (A) Representative H&E stains of well to moderately differentiated (left panel) and undifferentiated PDAC (right panel) from murine *PIK3CA$^{H1047R/+}$* (upper panel) or *Kras$^{G12D/+}$* (middle panel) samples and resected human PDAC specimens (lower panel). (B) Quantification of liver and lung metastasis of *Ptf1a$^{Cre/+}$;LSL-Kras$^{G12D/+}$* and *Ptf1a$^{Cre/+}$;LSL-PIK3CA$^{H1047R/+}$* mice (n=20 mice per genotype). Bar graph shows the percentage of mice with liver and lung metastases. (C) Analysis of activated Ras (Ras-GTP) in the pancreas of Ctrl, *PIK3CA$^{H1047R/+}$* and *Kras$^{G12D/+}$* mutant mice. (D) Analysis of activated Ras (Ras-GTP) and p110α expression levels in primary cells isolated from murine PDAC of indicated genotypes. (E) Serial staining of senescence-associated β-galactosidase (SA-β-Gal) expression and immunohistochemistry of PanINs from 6 month old *PIK3CA$^{H1047R/+}$* mutant mice. (F) qRT-PCR analysis of p16/Ink4a and p19/Arf mRNA expression in pancreata of 4 weeks old Ctrl and *PIK3CA$^{H1047R/+}$* mutant mice (left and middle panel). Representative immunohistochemistry of p16/Ink4a expression in PDAC of *PIK3CA$^{H1047R/+}$* mice (right panel). (G) Genetic strategy used to study the role of the *Cdkn2a* locus encoding p16/Ink4a and p19/Arf for p110α^{H1047R}-induced pancreatic carcinogenesis. (H) Kaplan-Meier survival analysis of the indicated conditional genotypes. `+` denotes the wild-type allele, `f` the conditional allele (n.s., not significant; *** p<0.001, log-rank test). (I) SA-β-Gal staining of PanINs from 2 month old compound mutant *PIK3CA$^{H1047R/+}$;Cdkn2a$^{f/f}$* (upper panel) and single mutant *PIK3CA$^{H1047R/+}$* (lower panel) mice. (J) Quantification of SA-β-Gal positive PanIN lesions of *Ptf1a$^{Cre/+}$;LSL-PIK3CA$^{H1047R/+}$* and *Ptf1a$^{Cre/+}$;LSL-PIK3CA$^{H1047R/+}$;Cdkn2a$^{f/f}$* mice (n= 3 per time point; 3 representative slides per mouse). Insets show representative lesions in high magnification. Scale bars, 50 μm for micrographs, 20 μm for insets. Error bars, ±SEM.

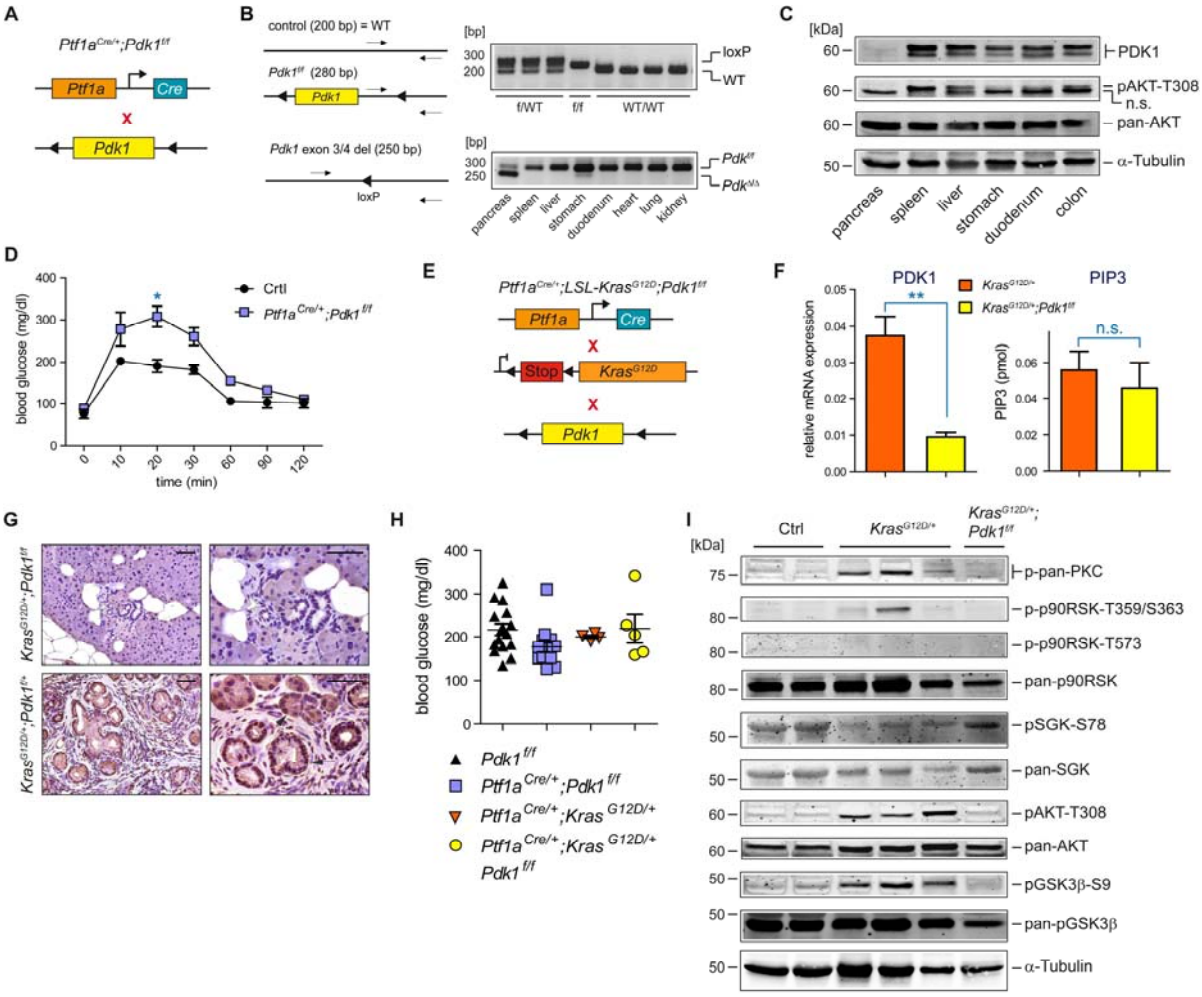

Figure S3, related to Figure 4. Ablation of *Pdk1* blocks Kras^{G12D}-driven PDAC formation. (A) Genetic strategy used to delete *Pdk1* in the pancreas. (B) Left panel: Genotyping strategy. Right panel: PCR analysis of tail tip DNA from wild-type (WT), heterozygous (f/+) and homozygous (f/f) conditional floxed *Pdk1* mice (upper panel). PCR analysis of DNA from the indicated organs shows *Ptf1a*^{Cre} mediated pancreas-specific deletion of exon 3/4 of *Pdk1* (*Pdk*$^{\Delta/\Delta}$) in *Ptf1a*$^{Cre/+}$;*Pdk1*$^{f/f}$ animals (lower panel). Sizes of wild-type and mutant PCR products are indicated. (C) Immunoblot analysis of PDK1 expression and PI3K/AKT pathway activation in indicated tissues of 3 month old *Ptf1a*$^{Cre/+}$;*Pdk1*$^{f/f}$ mice. α-Tubulin was used as loading control. n.s.: non specific band. (D) Glucose tolerance test of Ctrl and *Ptf1a*$^{Cre/+}$;*Pdk1*$^{f/f}$ mice fasted overnight (* $p<0.05$, Students t-test). (E) Genetic strategy used to study the cell-autonomous role of PDK1 signaling in Kras^{G12D}-driven pancreatic cancer formation. (F) qRT-PCR analysis of PDK1 mRNA expression in the pancreas of *Ptf1a*$^{Cre/+}$;*Kras*$^{G12D/+}$ and *Ptf1a*$^{Cre/+}$;*Kras*$^{G12D/+}$;*Pdk1*$^{f/f}$ mice (left panel; ** $p<0.01$, Students t-test) and analysis of the pancreatic PIP3 level of the indicated genotypes (right panel; n.s., not significant; Students t-test). (G) Immunohistochemical analysis of PDK1 expression in the pancreas of *Ptf1a*$^{Cre/+}$;*Kras*$^{G12D/+}$;*Pdk1*$^{f/f}$ (upper panel) and *Ptf1a*$^{Cre/+}$;*Kras*$^{G12D/+}$;*Pdk1*$^{f/+}$ (lower panel) pancreata. `+` denotes the wild-type allele, `f` the conditional allele. The arrowhead indicates an ADM and the arrow indicates a PanIN-1 lesion. (H) Blood glucose levels of 9-12 months old mice with the indicated genotypes in the fed state. (I) Immunoblot analysis of the phosphorylation state of PDK1 substrates in Ctrl, *Kras*$^{G12D/+}$ and *Kras*$^{G12D/+}$;*Pdk1*$^{f/f}$ mutant pancreata (age of all animals: 6 months). α-Tubulin was used as loading control. Scale bars, 50 μm. Error bars, ±SEM.

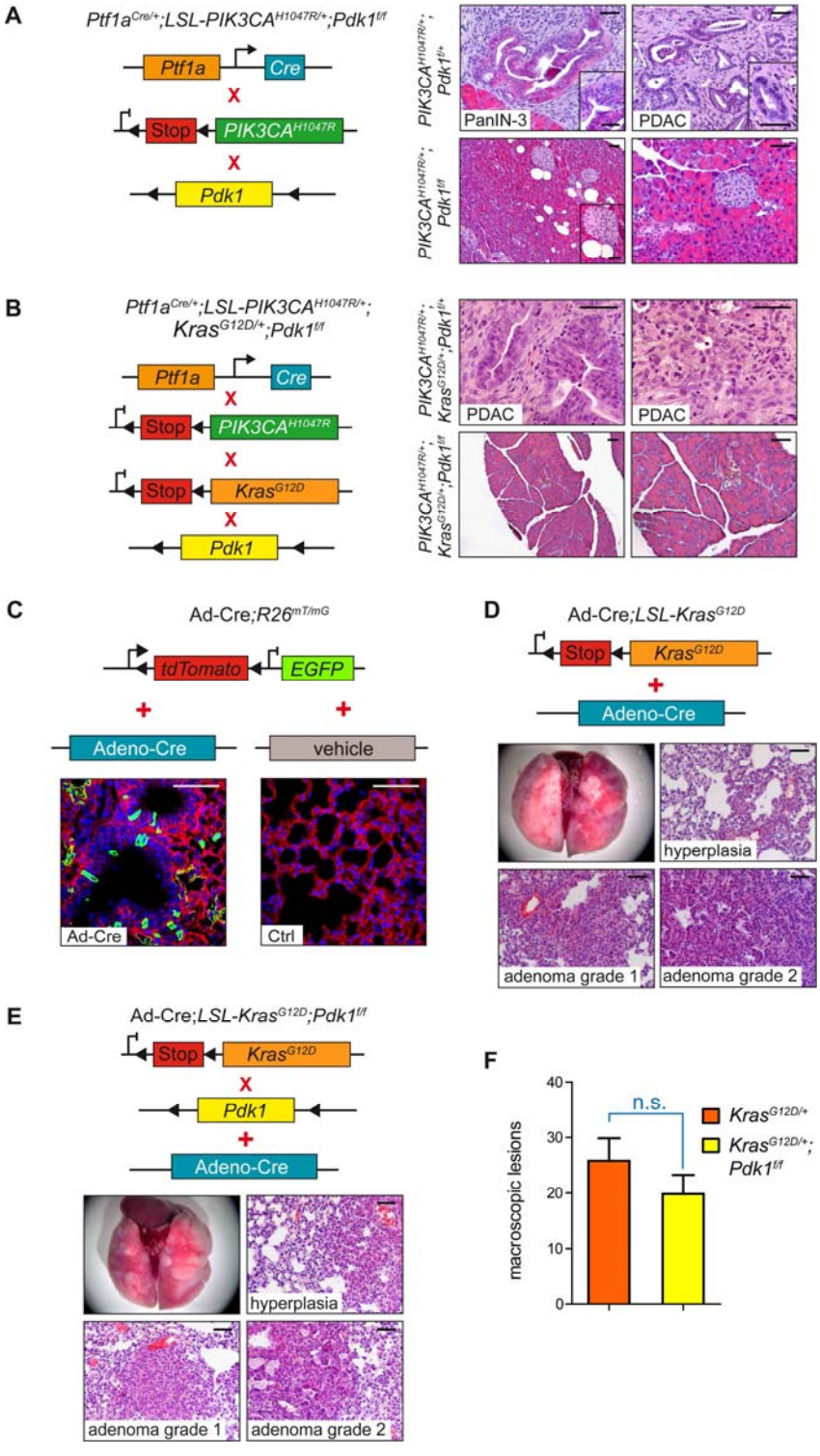
A
Ptf1a
Cre
Stop
PIK3CA
Pdk1
PanIN-3
PDAC
B
Kras
C
Ad-Cre;R26
tdTomato
EGFP
Adeno-Cre
vehicle
Ad-Cre
Ctrl
D
hyperplasia
adenoma grade 1
adenoma grade 2
E
F
n.s.
macroscopic lesions
40
30
20
10
0

Figure S4, related to Figure 5. PDK1 is dispensable for Kras^{G12D}-driven NSCLC. (A) Genetic strategy used to study the cell-autonomous role of the PI3K substrate PDK1 in p110α^{H1047R}-driven pancreatic cancer formation (left panel). Representative H&E stains of pancreata from the indicated genotypes (right panel). (B) Genetic strategy used to study the role of PDK1 in double mutant p110α^{H1047R};Kras^{G12D}-driven PDAC formation (left panel). Representative H&E stains of pancreata from the indicated genotypes (right panel). (C) Genetic strategy used to analyze adenoviral Cre (Ad-Cre) mediated recombination in the lung with a double fluorescent floxed tdTomato-EGFP reporter line (*R26$^{mT/mG}$*, upper panel). Confocal microscopic images of tdTomato (red) and Cre-induced EGFP (green) expression in the lung of Ad-Cre (lower left panel) or vehicle (lower right panel) treated animals. Nuclei were counterstained with TO-PRO-3 (blue). (D) Genetic strategy used to activate Kras^{G12D} expression in the lung by Adeno-Cre treatment (upper panel). Lower panel: Macroscopic view of multifocal lung tumors (upper left picture) and H&E stained representative microscopic lung sections graded according to the established 4-stage NSCLC grading system from a *LSL-Kras$^{G12D/+}$* mouse 8 weeks after Ad-Cre treatment. (E) Genetic strategy used to study the cell autonomous role of PDK1 in Kras^{G12D}-driven lung cancer formation (upper panel). Lower panel: Macroscopic view of multifocal lung tumors (upper left picture) and H&E stained representative microscopic lung sections graded according to the established 4-stage NSCLC grading system from a *LSL-Kras$^{G12D/+}$;Pdk1$^{f/f}$* mouse 8 weeks after Ad-Cre treatment. (F) Quantification of macroscopic lung lesions of Ad-Cre infected *LSL-Kras$^{G12D/+}$* and *LSL-Kras$^{G12D/+}$;Pdk1$^{f/f}$* mice (n.s., not significant, Students t-test). Insets show representative histology in high magnification. Scale bars, 50 μm for micrographs, 20 μm for insets. Error bars, ±SD.

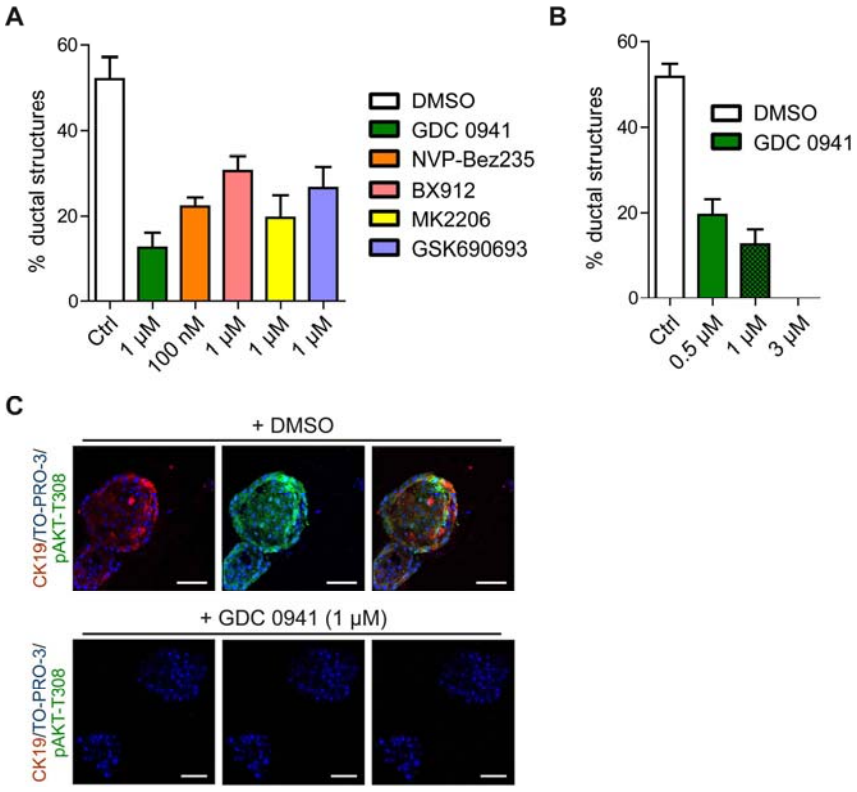

Figure S5, related to Figure 7. Human ADM depends on PI3K-PDK1-AKT signaling. (A) Quantification human ductal and acinar structures after 5 days in culture treated with TGFα (50 ng/ml) and the indicated chemicals. Bar graph shows percentage of ductal structures in the presence of TGFα. (B) Quantification of ductal and acinar structures treated with the indicated concentrations of GDC 0941 or vehicle (DMSO) after 5 days in culture. Bar graph shows percentage of ductal structures in the presence of 50 ng/ml TGFα. (C) Confocal microscopic images of TGFα-induced human ADM. Immunocytochemistry of CK19 expression (red) and phosphorylation of AKT-T308 (green) in ductal and acinar structures after 5 days of vehicle (DMSO, upper panel) or GDC 0941 (lower panel) treatment. Nuclei were counterstained with TO-PRO-3 (blue). Scale bars, 50 µm. Error bars, ±SEM.

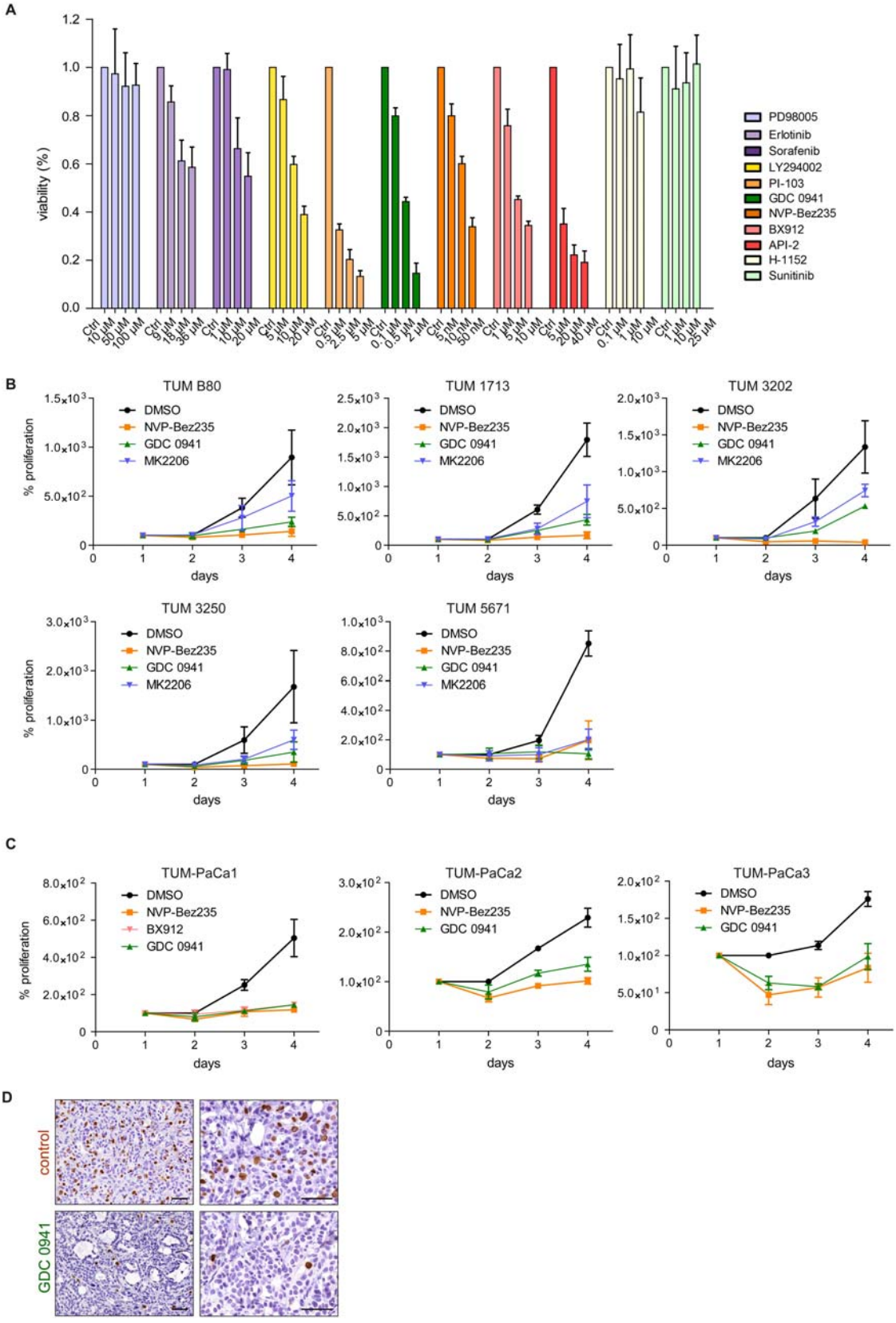
A
viability (%)
PD98005
Erlotinib
Sorafenib
LY294002
PI-103
GDC 0941
NVP-Bez235
BX912
API-2
H-1152
Sunitinib
B
TUM B80
TUM 1713
TUM 3202
TUM 3250
TUM 5671
% proliferation
days
DMSO
NVP-Bez235
GDC 0941
MK2206
C
TUM-PaCa1
TUM-PaCa2
TUM-PaCa3
BX912
D
control
GDC 0941

Figure S6, related to Figure 8. Inhibition of PI3K signaling blocks proliferation of primary Kras^{G12D}-driven murine and patient derived PDAC cells. (A) Dose dependent viability of primary murine Kras^{G12D}-driven PDAC cells after treatment with different targeted therapeutics was measured by MTT assay and compared to vehicle-treated controls. (B) Proliferation of different murine primary Kras^{G12D}-driven PDAC cells treated with the indicated chemicals. (C) Proliferation of different primary patient derived human PDAC cells treated with the indicated chemicals. (D) Immunohistochemical BrdU staining of representative xenotransplanted primary patient derived PDAC cells (see Figure 8G) treated with GDC 0941 or vehicle. Scale bars, 50 μm. Error bars, ±SEM.

Supplemental Experimental Procedures

Materials

The PDK1 inhibitor Bx912 (#1130) and the RSK inhibitor BI-D1870 (#1528) were purchased from Axon Medchem (Groningen, The Netherlands). The AKT inhibitors MK-2206 (#S1078) and GSK690693 (#S1113) were from Selleckchem (Houston, TX). PD98005 was purchased from Cell Signaling Technology (Danvers, MA). All other inhibitors used in this study (Erlotinib, Sorafenib, LY294002, GDC 0941, NVP-Bez235, and Sunitinib) were form LC Laboratories (Woburn, MA), or Tocris Bioscience, Bristol, UK (API-2, PI-103, and H-1152).

Construction of the targeting vector and generation of the *LSL-PIK3CA^{H1047R}* mouse line

Targeting the *Rosa26* locus by a knock-in strategy was performed on the basis of plasmid *pROSA26–1* as previously described (Seidler et al., 2008). A targeting vector containing a loxP-site flanked stop cassette with a neomycin resistance gene 5´ of the p110α^{H1047R} expression cassette was generated by standard cloning procedures (Figure S1A). The linearized targeting vector was electroporated into 129S6 embryonic stem (ES) cells. ES cells were selected with 200 µg/ml G418, and appropriately targeted clones were identified by PCR as described (Seidler et al., 2008). Correct recombination and single copy insertion was verified by Southern blot analysis with ^{32}P-labeled 5' external probe and internal probe for the neomycin resistance gene, respectively (Figure S1B). Germ-line transmission was achieved in 2/2 clones harboring the targeted allele. A three-primer PCR strategy (Figure S1C) was used to genotype animals as described (Seidler et al., 2008).

Histochemistry, immunohistochemistry and SA-β-galactosidase staining

For histopathological analysis, murine and human tissue specimens were fixed in 4% buffered formalin, embedded in paraffin and sectioned (3 µm thick). For quantification and grading of murine ADM and PanIN, three slides per mouse and 3 mice per time point were analyzed according to the established nomenclature for the grading of PanIN lesions in mice (Hruban et al., 2006). Alcian blue staining was performed on paraffin embedded tissue sections using an aqueous alcian blue solution (pH 2.5) and counterstaining using nuclear fast red. For immunodetection, formalin-fixed paraffin-embedded tissue sections and in-house prepared tissue microarrays were

dewaxed and placed in a microwave (10 min., 600 watt) to recover antigens before incubation with primary antibodies: pAKT-T308 (#2965; 1:50); pAKT-S473 (#4060; 1:50); pGSK3β–S9 (#9323; 1:100); PDK1 (#3062; 1:50; all from Cell Signaling Technology); CK19 (TROMAIII; 1:100; Developmental Studies Hybridoma Bank, Iowa City, IA); p16 (sc-1661; 1:100), p21 (sc-397-G; 1:100; both from Santa Cruz Biotechnology, Santa Cruz, CA), p53 (CM5; 1:100; Novocastra/Leica Mikrosysteme, Wetzlar, Germany), Muc5 (Muc5AC, clone 45M1, 1:200; Neomarkers, Fremont, CA) and BrdU (MCA2060; 1:250; AbD Serotec, Düsseldorf, Germany). Primary antibodies were followed by secondary antibodies conjugated to biotin (Vector Laboratories, Burlingame, CA). Senescence-associated β-galactosidase staining was performed on cryo-sections with the Senescence β-Galactosidase Staining Kit (Cell Signaling Technology) according to the manufacturer's protocol.

Stereomicroscopy and quantification of metastasis frequency

Macroscopic pictures of murine PDAC and metastases were taken by using a Zeiss Stemi 11 stereomicroscope. At necropsy, murine organs were investigated macroscopically for metastases. For microscopic analysis at least four series of sections (200 µm between series) of paraffin embedded lungs and livers of 20 mice per genotype with PDAC were prepared and stained using H&E. Lung and liver sections were microscopically investigated for the presence of metastases.

Preparation of total cell lysates and immunoblotting

Whole-cell lysates were prepared as described (von Burstin et al., 2009; von Burstin et al., 2008). For protein isolation from mouse, human and xenografted human tissues, a piece of tissue was removed, placed in immunoprecipitation buffer and homogenized. Proteins were resolved on SDS-polyacrylamide gels, transferred to polyvinylidene difluoride membranes, and incubated overnight at 4°C with primary antibodies: p110α (#4249), pAKT-T308 (#2965), pAKT-S473 (#4060), pan-AKT (#4691), pGSK3β-S9 (#9323), pan-GSK3β (#9315), pPDK1-S241 (#3061), PDK1 (#3062), p-pan-PKC (#9371), pSGK-S78 (#3271), pan-SGK (#3272), p-p90RSK-T573 (#9346), p-p90RSK T359/S363 (#9344) and RSK 1/2/3 (#9355; all from Cell Signalling Technology), β-actin (#A5316) and α-Tubulin (#T9026; both from Sigma-Aldrich). Proteins recognized by the antibodies were detected by the Odyssey Infrared Imaging System (Licor, Bad Homburg, Germany) using Alexa680-coupled

(Molecular Probes, Leiden, The Netherlands), or IRDeye800-coupled (Rockland, Gilbertsville, PA) secondary antibodies.

PIP3 assay

Isolation and detection of phosphatidylinositol (3,4,5)-triphosphate (PIP3) levels in murine pancreata was performed with the PIP3 Mass Elisa Kit (K-2500s, Echelon, Salt Lake City, UT). For isolation of PIP3 from the pancreas of 6 weeks old mice, about one third of the pancreas was excised, weighed and homogenized in 0.5 M trichloroacetic acid and isolated according to the manufacturer's protocol. PIP3 levels were adjusted to input weight of the tissue.

Ras activation assay

Tissue and cell line samples were lysed in MLB-buffer (Millipore, Schwalbach, Germany) supplemented with 10% glycerol (Sigma-Aldrich), phosphatase-inhibitor (Serva, Heidelberg, Germany) and protease-inhibitor (Roche, Mannheim, Germany). Cleared lysates were normalized for protein and 1 mg of each sample was incubated with Raf-RBD Protein GST beads (Cytoskeleton, Dever, Co) at 4°C for 2 hours with rotation. Beads were pelleted, washed twice, resuspended in Lämmli buffer, heated and run on a 12% SDS-gel. Transfer to a polyvinylidene difluoride membrane and detection of pulled activated Ras with a pan-Ras antibody (Millipore) was performed as described above.

Acinar cell preparation and acinar to ductal metaplasia (ADM) assay

Pancreatic acinar cells were isolated from *Ptf1a*$^{Cre/+}$;*Kras*$^{G12D/+}$ and *Ptf1a*$^{Cre/+}$;*Kras*$^{G12D/+}$;*Pdk1*$^{f/f}$ compound mutant pancreata as described by Means et *al.* (Means et al., 2005). Human primary acinar cells were isolated from normal human pancreas obtained from surgical resections for malignant disease. Isolated acini were cultured in ACL-3 medium (Conradt et al., 2011). Acinar cells were treated with and without 50 ng/ml TGFα (Sigma) and GDC 0941 (pan class I PI3K inhibitor), NVP-Bez235 (dual PI3K-mTOR inhibitor), BX912 (PDK1 inhibitor), MK2206 (AKT inhibitor), GSK690693 (AKT inhibitor), BI-D1870 (RSK inhibitor), or vehicle (DMSO). Acinar and ductal structures were counted after 5 days treatment.

Quantitative reverse-transcriptase PCR

Total RNA was isolated from tissues and cell lines using the RNeasy kit (Qiagen, Hilden, Germany) following the manufacturer's instructions. Quantitative mRNA analysis were performed using real-time PCR analysis (TaqMan, PE Applied Biosystems, Norwalk, CT) and standard curves as previously described (Saur et al., 2005).

qRT-PCR Primers

Species	**Transcript**	**Primer name**	**Sequence (5´ - 3´)**
mouse	Pdk1	Pdk1 forward	ACGCCCTGAAGACTTCAAGTTTG
		Pdk1 reverse	GCCAGTTCTCGGGCCAGA
mouse	p16/Ink4a	p16 forward	CCCAACGCCCCGAACT
		p16 reverse	GTGAACGTTGCCCATCATCA
mouse	p19/Arf	p19 forward	TCGCAGGTTCTTGGTCACTGT
		p19 reverse	GAACTTCACCAAGAAAACCCTCTCT

Genotyping Primers

Primer name	**Sequence (5´ - 3´)**
R26-PIK3CA^{H1047R} Common forward	AAAGTCGCTCTGAGTTGTTAT
R26-PIK3CA^{H1047R} MUT reverse	GCGAAGAGTTTGTCCTCAACC
R26-PIK3CA^{H1047R} WT reverse	GGAGCGGGAGAAATGGATATG
R26-PIK3CA^{H1047R} Common forward	AAAGTCGCTCTGAGTTGTTAT
R26-PIK3CA^{H1047R} Recombined reverse	AGCCGAAGGTCACAAAGTC
Pdk1 forward	ATCCCAAGTTACTGAGTTGTGTTGGAAG

Pdk1 Common reverse	TGTGGACAAACAGCAATGAACATACACGC
Pdk1 Recombined forward	CTATGCTGTGTTACTTCTTGGTGCACAG
Pdk1 Common reverse	TGTGGACAAACAGCAATGAACATACACGC
Craf forward	TGGCTGTGCCCTTGGAACCTCAGCACC
Craf Common reverse	AACATGAAGTGGTGTTCTCCGGGCGCC
Craf Recombined forward	ATGCACTGAAATGAAAACGTGAAGACGACG
Craf Common reverse	AACATGAAGTGGTGTTCTCCGGGCGCC

β-galactosidase staining

β-galactosidase staining of whole tissues and cryosections was performed as previously described (Mayr et al., 2008; Seidler et al., 2008). Stereoscopic pictures were taken using a Zeiss Stemi 11 microscope. For histological analysis, organs were cryosectioned after fixation, postfixed in 0.2% glutaraldehyde in PBS and stained as described above. Counterstaining was done with eosin or nuclear fast red.

Adenovirus infection

Infection of lungs with 1 x 10^7 PFU Ad-Cre (University of Iowa, IA) was performed as described (DuPage et al., 2009).

Blood glucose level determination

Blood glucose levels were measured with a glucometer (Abbott Laboratories, Wiesbaden, Germany) by standard procedures.

Glucose tolerance test (GTT)

After an overnight fast, GTTs were performed by intra-peritoneal injection of 1.5 g/kg body weight of glucose (Sigma-Aldrich). Blood samples were taken at 0-, 10-, 20-,

30-, 60-, and 120-min time points and glucose levels measured with a glucometer (Abbott Laboratories).

Supplemental References

DuPage, M., Dooley, A.L., and Jacks, T. (2009). Conditional mouse lung cancer models using adenoviral or lentiviral delivery of Cre recombinase. Nat Protoc *4*, 1064-1072.

Mayr, U., von Werder, A., Seidler, B., Reindl, W., Bajbouj, M., Schmid, R.M., Schneider, G., and Saur, D. (2008). RCAS-mediated retroviral gene delivery: a versatile tool for the study of gene function in a mouse model of pancreatic cancer. Hum Gene Ther *19*, 896-906.

Saur, D., Seidler, B., Schneider, G., Algul, H., Beck, R., Senekowitsch-Schmidtke, R., Schwaiger, M., and Schmid, R.M. (2005). CXCR4 expression increases liver and lung metastasis in a mouse model of pancreatic cancer. Gastroenterology *129*, 1237-1250.